ADVANCED OPTICAL MATERIALS
www.advopticalmat.de

Layer-Dependent Dielectric Function of Wafer-Scale 2D MoS_2

Baokun Song, Honggang Gu, Mingsheng Fang, Xiuguo Chen, Hao Jiang, Renyan Wang, Tianyou Zhai, Yen-Teng Ho,* and Shiyuan Liu**

Wafer-scale, high-quality, and layer-controlled 2D MoS_2 films on *c*-sapphire are synthesized by an innovative two-step method. The dielectric functions of MoS_2 ranging from the monolayer to the bulk are investigated by spectroscopic ellipsometry over an ultra-broadband (0.73–6.42 eV). Up to five critical points (CPs) in the dielectric function spectra are precisely distinguished by CP analysis, and their physical origins are identified in the band structures with the help of first-principles calculations. Results demonstrate that the center energies of these CPs exhibit intriguing layer dependency, which are interpreted by the intrinsic layer-dependent transitions in MoS_2. Specially, the change in the imaginary part of the dielectric functions versus the thickness exhibits a "W" like curve, and the two valley bottoms appear at about four-layer and 10-layer respectively. These complex fluctuations are attributed to the alternating domination of the decreasing excitonic effect, the increasing joint density of states, and the mass density increase in relative thick MoS_2 samples.

1. Introduction

In recent years, 2D MoS_2 has ignited intensive interest due to the gradually widespread applications in nanoelectronics, optoelectronics, and spintronics.[1–5] Various MoS_2-based devices with exotic performances, such as photoelectric detector,[1,6] field effect transistor,[1,7] solar cell,[8] sensor,[5] and energy storage devices,[9] have been developed, benefiting from the layer-dependent bandgap,[10] valley selective circular dichroism,[11] high on/off ratio,[12] and high thermostability[12] of the 2D MoS_2. The performance of these novel devices significantly depends on the intrinsic optical properties (especially the dielectric function) of the 2D MoS_2, which exhibit an intriguing layer dependency due to the enhanced quantum confinement effect and the absence of inversion symmetry. Therefore, the effective characterization of the layer-dependent optical properties of MoS_2 is critical for the performance improvement and the optimal design of those photoelectric devices based on MoS_2.

Layer-dependent optical properties of MoS_2, including absorbance,[1] photoluminescence spectra,[10] Raman spectra,[13] and second-harmonic generation effect,[14] have been measured and discussed previously. However, these studies can hardly gain the basic optical constants, such as dielectric function, complex refraction index, etc., which play an important role in the quantitative design and optimization of those MoS_2-based photoelectric devices.[15] Beyond these researches, there are also some reports on the dielectric function of the 2D MoS_2, where the techniques they used can be roughly divided into three types: ellipsometry,[16–26] reflection (or absorption) spectrum method,[27,28] and contrast spectrum or differential reflection (or transmission) spectrum method.[29,30] By using of ellipsometry, Li et al. investigated the optical properties of the monolayer and bulk MoS_2, and identified some critical points (CPs) in their dielectric function spectra.[22] The frequency-dependent reflection (transmission) spectra and corresponding differential spectra of the monolayer MoS_2 were simultaneously measured by Morozov et al., then the dielectric function was extracted.[27] Li et al. measured the reflection spectra of the mechanical exfoliation monolayer MoS_2 flake and the bulk MoS_2, then their dielectric functions were calculated combined with a Kramers–Kronig constrained variational analysis.[28] Nevertheless, these published experimental reports on the dielectric function of MoS_2 mainly focus on the monolayer and bulk counterpart and the spectral range is relatively narrow. Apart from these experimental studies, some researchers have also devoted to predict the dielectric properties of the 2D MoS_2 with the help of theoretical calculations.[31,32] For example, Johari et al. studied the dielectric properties of monolayer, bilayer, and bulk MoS_2 by computing the electron

B. K. Song, Dr. H. G. Gu, M. S. Fang, Dr. X. G. Chen, Dr. H. Jiang, Prof. S. Y. Liu
State Key Laboratory of Digital Manufacturing Equipment and Technology
Huazhong University of Science and Technology
Wuhan 430074, Hubei, China
E-mail: shyliu@hust.edu.cn

R. Y. Wang, Prof. T. Y. Zhai
State Key Laboratory of Material Processing and Die and Mould Technology
Huazhong University of Science and Technology
Wuhan 430074, Hubei, China
E-mail: zhaity@hust.edu.cn

Prof. Y.-T. Ho
Department of Materials Science and Engineering
National Chiao Tung University
Hsinchu 30010, Taiwan, China
E-mail: 9418813@gmail.com

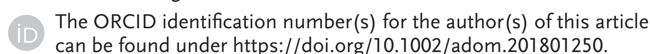
The ORCID identification number(s) for the author(s) of this article can be found under https://doi.org/10.1002/adom.201801250.

DOI: 10.1002/adom.201801250

© 2018 WILEY-VCH Verlag GmbH & Co. KGaA, Weinheim

energy loss spectrum using first-principles calculations.[31] On the basic of the first-principle calculations, Kumar and Ahluwalia systematically studied the influence of layer number on the dielectric properties of the MoS_2 for in-plane as well as out-of-plane polarization.[32] Due to the lack of sufficient high-quality and layer-controlled 2D MoS_2, the layer-dependent dielectric function of MoS_2 has yet to be studied adequately from the perspective of experiment, and several existing literatures relevant to this theme have been controversial thus far.[16–18]

The existing preparation techniques of 2D MoS_2, such as chemical vapor deposition (CVD),[33,34] mechanical exfoliation,[35] liquid phase exfoliation,[36] and hydrothermal,[37] have their own advantages and disadvantages.[38] For example, CVD method can synthesize large-area 2D MoS_2, but it is difficult to prepare MoS_2 with specified layers directly.[39] Multilayer films obtained from the repeated transfer of the monolayer MoS_2 may contain a buffer layer between two adjacent MoS_2 layers, which will affect the optical properties of MoS_2 and reduce the performance of the related devices.[40,41] Exfoliation (including mechanical exfoliation and liquid phase exfoliation) processes are conventional methods to prepare high-quality MoS_2 flakes in laboratory, while these MoS_2 flakes with only micron-scale lateral sizes and highly random thicknesses are not suitable for the investigation of the layer-dependent properties.[42] 2D MoS_2 films prepared by other processes also face similar dilemmas, including small area, poor crystalline quality, and uncontrollable layer number. Therefore, the preparation of the large-area, high-quality, and layer-controllable 2D MoS_2 is the key to investigating the optical properties of MoS_2 comprehensively.

In this work, an innovative two-step method is proposed to synthesize wafer-scale and high-quality 2D MoS_2 films, where the layer number of the MoS_2 film can be controlled precisely by adjusting the deposition thickness of the precursor material MoO_3. The two-step method overcomes most of the dilemmas that prior preparation processes are suffering from, such as limited area, poor crystalline quality, and lack of scalability. Benefiting from the layer-controlled and high-quality MoS_2 films prepared by this innovation method, we comprehensively investigate the dielectric function evolution in MoS_2 ranging from the monolayer to the bulk by spectroscopic ellipsometry (SE) over an ultra-broadband (0.73–6.42 eV). With the help of the CP analysis method, up to five CPs (A–E) in the dielectric function spectra are distinguished precisely and their physical mechanisms are revealed combined with the first-principles calculations. The imaginary part of the dielectric functions at these CPs exhibits a "W" like curve versus the thickness, and the two valley bottoms appear at about four-layer and 10-layer. We explain these complex fluctuations as an integrated impact and competition of the layer-dependent decreasing excitonic effect,[43] the layer-dependent increasing joint density of states (JDOS),[44] and the mass density increase in relative thick MoS_2 specimens.[45]

2. Results and Discussion

Figure 1 illustrates the schematic diagram of the two-step method proposed by us. The first step is the deposition of precursor material MoO_3 on the *c*-sapphire by E-gun. Compared with the MoO_3 films prepared by other deposition methods, such as sputtering and pulsed laser deposition,[46] the MoO_3 film deposited by E-gun exhibits larger area, high uniformity, and adjustable thickness, which guarantees the synthesis of wafer-scale and high-quality MoS_2 films in the second step. The second step is the sulfurization process of MoO_3 by H_2S and Ar gaseous mixture. It is worth mentioning that the reactant gaseous hydrogen sulfide is more reactive and easier to control compared with the commonly used gaseous sulfur, which ensures the sufficient sulfurization of MoO_3 and effectively improves the purity of the target product MoS_2.

Figure 2a is the optical picture of a three-layer MoS_2 film on a 2 in. *c*-sapphire wafer, and the ultrauniform optical contrast suggests the high uniformity of the MoS_2 film over the entire wafer. Figure 2b presents the measured and the best matched X-ray photoelectron spectroscopy (XPS) results of the three-layer MoS_2 film. It shows that the center energies of these XPS peaks agree well with the theoretical binding energies of the corresponding orbital electrons of Mo and S elements. Further, both the Mo $3d_{5/2}$ and the Mo $3d_{3/2}$ features presented in Figure 2b are deconvoluted with only one Voigt function, indicating that only one molybdenum-containing chemical species exists at the surface. The same analysis can be applied to the sulfur atoms as illustrated in Figure 2c. The mole ratio of S and Mo atoms approximately equals to the theoretical value of 2, which is determined from the ratio of the peak areas of S 2p and Mo 3d. All the above analysis verifies the successful synthesis of 2D MoS_2 films. To further check the crystal quality of the MoS_2 film, Raman spectra of five points distributed along the diameter direction evenly on the MoS_2 wafer are measured, which are uniformly plotted in Figure 2d. The specific Raman detection positions on the three-layer 2D MoS_2 wafer have been marked out in the optical picture as shown in Figure 2a. The widths of Raman peaks A_{1g} and $E_{2g}{}^1$ are about 7 and 8 cm^{-1} and consistent with those of mechanical exfoliated MoS_2 flakes,[47] indicating that the MoS_2 film prepared by the two-step method has high crystal quality. As presented in Figure 2e, the frequency

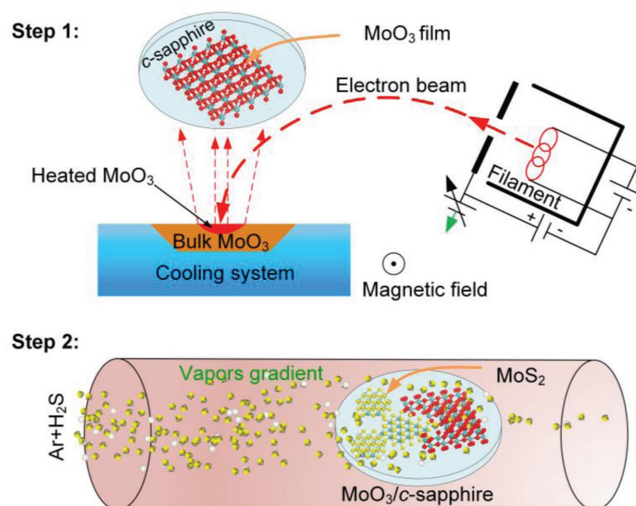

Figure 1. Schematic diagram of the two-step method. Step1: deposition of MoO_3 on *c*-sapphire; Step2: sulfurization process of MoO_3 by H_2S and Ar gaseous mixture.

 © 2018 WILEY-VCH Verlag GmbH & Co. KGaA, Weinheim

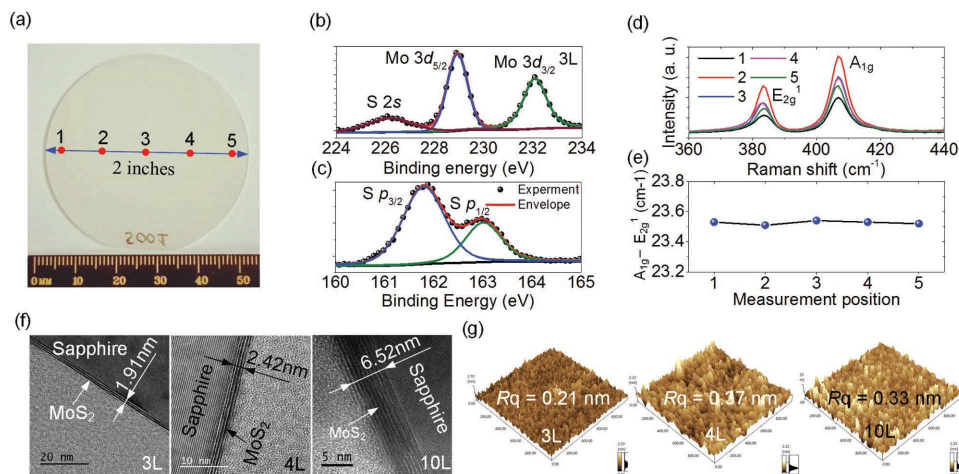

Figure 2. a) Optical picture of three-layer MoS_2 film on the 2 in. *c*-sapphire wafer. b,c) Measured XPS spectra and corresponding peak-differentiation-imitating analysis for the three-layer MoS_2 film. d) Raman spectra of five points along the diameter of the three-layer MoS_2 wafer. e) Frequency differences between the A_{1g} peak and E_{2g}^1 peak. f,g) The thicknesses and surface roughness of three-, four-, and 10-layer MoS_2 films determined by TEM and AFM.

differences between peaks A_{1g} and E_{2g}^1 are nearly independent of the detection positions on the MoS_2 wafer confirming that the MoS_2 film is very uniform over the MoS_2 wafer. Moreover, the frequency difference of Raman peaks E_{2g}^1 and A_{1g} is usually considered as an index to identify the layer number of the MoS_2 film. In our MoS_2 wafer, the frequency differences between the two Raman peaks A_{1g} and E_{2g}^1 for the five tested points are stable at around 23.5 cm^{-1} and consistent with that of the three-layer MoS_2 fabricated by Liu et al.[47] The surface condition and the layer number of the MoS_2 films are also checked by the atomic force microscope (AFM) and TEM. As indicated in Figure 2f,g, the extremely low surface roughness and clear stratified structure suggest that the MoS_2 films prepared by the two-step method are layer controlled with rather smooth surface. AFM results of the MoS_2 films with other layers can be found in Figure S1 in the Supporting Information.

The dielectric functions and the thicknesses of these MoS_2 specimens have been determined by analyzing the ellipsometric spectra with a nonlinear regressive fitting method. In the ellipsometric analysis, an multilayer stacking model is established to describe the optical structure of the 2D MoS_2 samples as shown in Figure S3 in the Supporting Information, and the dielectric functions of MoS_2 are parameterized by a physical dispersive model which is a combination of classical oscillators. Details about the ellipsometric analysis can be found in the Supporting Information. The measured and best-fitting ellipsometric spectra have been shown in Figure S4 in the Supporting Information. The thicknesses of the MoS_2 films determined by TEM, AFM, and SE are summarized in **Table 1** and have good consistency with each other. Compared with the AFM and TEM results, the thicknesses determined by the SE appear slightly smaller, which can be interpreted as our unique consideration of the Bruggeman interlayer (Figure S3, Supporting Information) in the SE analysis. Actually, the existence of the interlayer can be confirmed from the relatively fuzzy interfaces between the MoS_2 film and the *c*-sapphire substrate as presented by the TEM pictures as shown in Figure 2f. Comparing with those prior ellipsometric analysis to the 2D MoS_2,[22,25,27,28] the application of the Bruggeman interlayer in the optical model of the MoS_2 specimen can promote the goodness of the ellipsometric fit effectively.[48,49] The layer number shown in the first column of Table 1 is an approximation of the thicknesses divided by the nominal interlayer spacing (6.15 Å) of the MoS_2 bulk.[50]

Figure 3 illustrates the dielectric functions of the MoS_2 films with different layers determined by the SE. The results in our study agree well with those in publications,[20,22] but cover a much broader band and involve more samples with the thickness ranging from a monolayer to the bulk, which will help us to more comprehensively investigate the optical properties of MoS_2. Benefiting from the broader energy band, up to five CPs can be observed in the dielectric functions of the MoS_2, which are labeled with uppercase letters A–E as shown in Figure 3b. Each CP corresponds to a specific band transition in the band structure of MoS_2. To interpret the physical origins of these CPs, we calculate the band structure of MoS_2 by using the Vienna Ab initio Simulation Package. Taking the monolayer MoS_2 as an example, the corresponding positions of the CPs have been marked in the band structure as shown in Figure 3c. The direct-gap transitions between the maxima of the split valence bands (V_1 and V_1') and the minimum of the conduction band (C_1) lead to the formations of the CPs A and B. The valance bands splitting at the K point of the Brillouin zone (BZ)

Table 1. A summary of thicknesses of the MoS_2 samples measured by TEM, AFM, and SE.

Layer number		1L	3L	4L	6L	8L	10L	13L
Thickness [nm]	TEM		1.91	2.42		5.20	6.52	
	AFM	0.66			3.65	4.84	6.80	8.67
	SE	0.60	1.89	2.40	3.53	4.74	6.01	8.15
	Interlayer[a)]	0.10	0.63	0.64	0.62	0.74	0.82	0.72

[a)]A Bruggeman interlayer between the MoS_2 film and the *c*-sapphire.

 © 2018 WILEY-VCH Verlag GmbH & Co. KGaA, Weinheim

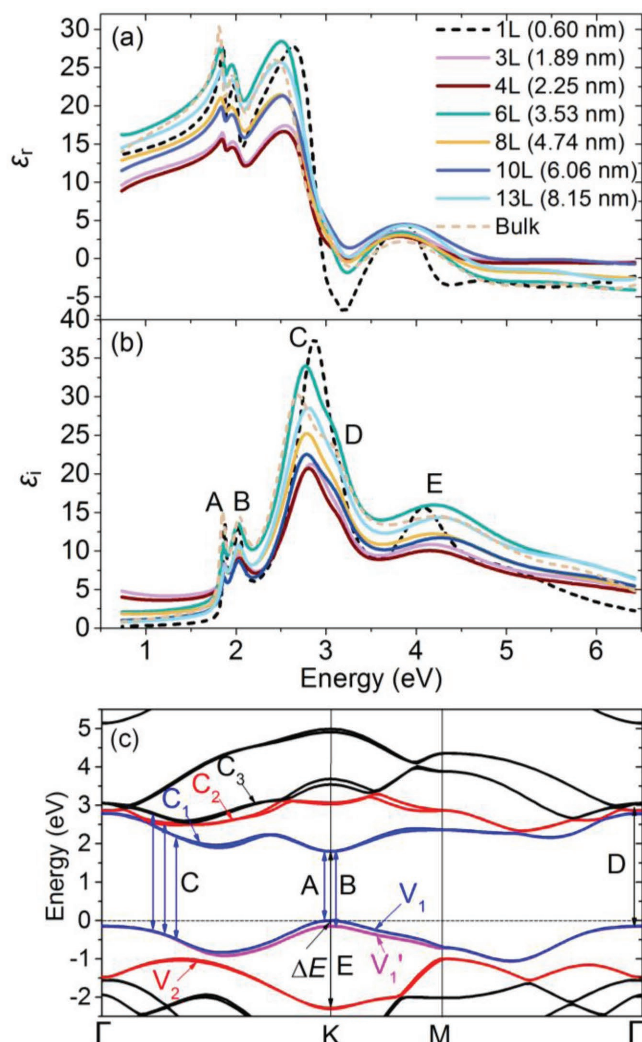

Figure 3. Dielectric functions of MoS_2 samples. a) Real part. b) Imaginary part. c) The quasiparticle band structure of the monolayer MoS_2.

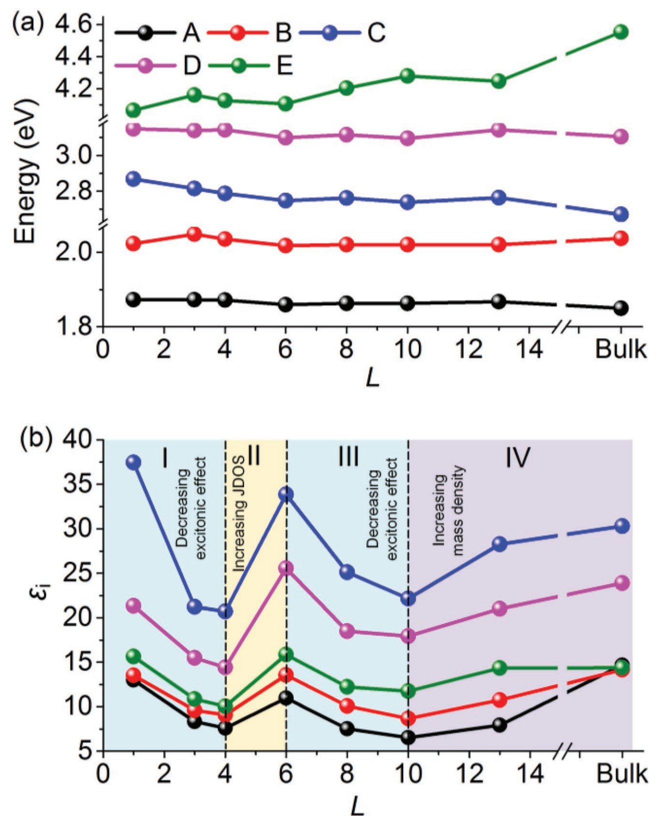

Figure 4. a) The energy positions of CPs (A–E) versus the layer number L of MoS_2. b) The imaginary part ε_i of the dielectric function at the CPs versus L.

can be interpreted mainly as the intralayer spin–orbit coupling (SOC) effect, which is partly caused by the breaking of inversion symmetry.[51–53] The splitting value ΔE is about 150 meV, which also corresponds to the center energy difference between the CPs A and B as shown later. The CP C corresponds to the complex many-body effects that occur between the K and Γ points of the BZ. Specifically, it may be associated with the six nearly degenerate exciton states made from transitions between V_1 and the first three lowest conduction bands (C_{1-3}).[54] The broad CP C can be understood from the fact that the electronic states between the K and Γ points contain mostly contributions from the nonlocalized p orbitals character of the sulfur atoms.[55] The electron transitions from V_1 to C_{1-3} around Γ point in the BZ give rise to the CP D. It should be noted that the valance and conduction bands involved in the electron transitions of the CPs C and D are of the same type except that the transition positions are different. The direct transitions from V_2 to C_1 occurring at the K point of the BZ make a major contribution to the formation of the CP E. Above the CP E, there exists a rarely reported higher energy CP at 5.8 eV, and its physical causes have not yet been explained unambiguously. We conjecture it may be relevant to the optical transitions from V_1 to higher conduction bands. It is worthy pointing out that although the band structures of monolayer MoS_2 and multilayer MoS_2 are slightly different, the formation mechanisms of their CPs are analogous to each other.

These CPs marked in Figure 3b are only distinguished in the dielectric function spectra by a superficial observation without rigorous theoretical support. Therefore, the CP analysis method is introduced to further identify these CPs more accurately from the uninteresting background responds.[22,44] By using this method, the center energies as well as the shapes of these CPs can be totally determined. More details about the CP analysis method and the results have been shown in the "CP analysis method" part of the Supporting Information. **Figure 4** presents the changes of the center energies (E_0) and the values of imaginary part (ε_i) of the dielectric function at these CPs versus the MoS_2 thickness (in the form of layer number L). It can be observed from the E_0–L curves as shown in Figure 4a that the positions of the split CPs A and B are remarkably stable with respect to the layer number of MoS_2 except for the bulk sample, and there remains a splitting values (about 150–180 meV) between A and B. This can be explained as the fact that with the thickness increasing, the change in the quasiparticle bandgap almost cancels out the change in the excitonic binding energy.[51,56] Actually, the splitting values between the CPs A and B in the MoS_2 are dominated by the intralayer

© 2018 WILEY-VCH Verlag GmbH & Co. KGaA, Weinheim

SOC effect, which is insensitive to the layer number, though the layer-coupling effect is obvious for multilayer MoS_2.[57] The slightly larger splitting value in the bulk MoS_2 may be due to an additional split caused by the interlayer interaction. Similar to A and B, there is a layer-independent difference value (about 320–380 meV) between the center energies of the CPs C and D except for the monolayer and bulk samples. This may be due to that the energy gap between the V_1 and C_1 at Γ point (for the CP D) is wider than that at Γ–K (for the CP C), resulting in the energy gap is layer independent. This phenomenon also confirms that the quasiparticle behaviors at the CPs C and D are similar to each other. In the monolayer MoS_2, the smaller splitting value between the CPs C and D can be partly attributed to the absence of the interlayer interaction, while the slightly stronger interlayer interaction in bulk MoS_2 enlarges this split. Different from A and B, the positions (i.e., center energies) of the CPs C and D appear a slightly red-shift with the layer number increasing, which can be posed by the weakening of excitonic effect arising from the enhanced dielectric shielding. On the contrary, the CP E exhibits an obvious blue-shift when the layer number increases.

The magnitudes of ε_i at the above CPs have been drawn uniformly in Figure 4b as functions of the layer number L. It can be seen that the ε_i–L curve exhibits an obvious "W" shape, and the two valley bottoms appear at the layer numbers of about 4 and 10, respectively. The alternating domination of the layer-dependent decrease of the excitonic effect, the layer-dependent increase of the JDOS, and the slight mass density increase in the multilayer and bulk MoS_2 leads to the complex fluctuations in the dielectric function versus the thickness. For a system under thermal equilibrium, the magnitude of the excitonic effect can be represented by the exciton binding energy $E^n{}_b = \mu e^4/2[\hbar\varepsilon_n(n-1/2)]^2$ to some extent.[43] Here n denotes the quantum number; μ, $\hbar$, and ε_n refer to the reduced mass of the exciton, the reduced Planck constant, and the dielectric function experienced by the nth excitons, respectively. For excitons at a specific energy level, the excitonic effect will decrease with the increase of ε_n. Considering that the magnitude of ε_n is positive correlated with the thickness of shielding materials (here is the 2D materials), we deduce that the excitonic effect decreases as the layer number of MoS_2 increases. The JDOS represents the density of paired initial–final states that can participate in the optical transition with a certain energy.[58] Contrary to the layer-dependent decrease of the excitonic effect, the JDOS exhibits a layer-dependent increase. However, its acceleration gradually decreases and eventually approaches zero. The last factor that can influence the dielectric properties of the MoS_2 is the mass density. The dielectric function will increase as the mass density increases. The mass density plays a remarkable role only in the multilayer (>10 layers for MoS_2) films and bulk materials. For MoS_2 films below 10 layers, the difference in mass density can be neglected.

As shown in Figure 4b, the first valley in the ε_i–L curves covers the layer range from 1 to 6, which is the result of the competition between the excitonic effect and the JDOS. Specifically, when L is less than 4 (region I), the weakened excitonic effect gives rise to the decrease of ε_i. However, due to the increase of the JDOS, the optical transition rapidly offsets the decaying excitonic effect and dominates the change in ε_i when L is between 4 and 6 (region II). The bottom of the first valley appears when the layer number is about 4, where the decreasing rate of exciton effect and the increasing rate of optical transition reach a balance. The physical origin of the second valley that spans over the layer number from 6 to 12 can be attributed to the continuation of the mentioned competition between the excitonic effect and the JDOS as well as combined the influence of the gradually increasing mass density. When L is between 6 and 10 (region III), the dielectric shielding effect is further enhanced and the excitonic effect disappears gradually, while the growth rate of JDOS resulting from the thickening of the MoS_2 slows down and eventually tends to be zero. The decaying excitonic effect once again plays a major role in the dielectric properties of MoS_2. Actually, the turning point located at the layer number of 6 also implies that the decreasing rate of excitonic effect transcends the growth rate of JDOS again. It is worth mentioning that the influence of the increasing mass density is not significant in region III. In regions I and III, although the excitonic effect plays a leading role in the dielectric function, the degrees of influence are different. The flatter curve in region III indicates that decreasing rate of the excitonic effect is not as high as that in region I. When L is larger than 10 (region IV), the excitonic effect and the optical transition in this region are extremely weak, and the slight uptrend in ε_i can be interpreted as the mass density increase of the multilayer and bulk MoS_2.[45] Namely, as the layer number of MoS_2 increases, the mass density slightly increases, and the dielectric functions of multilayer MoS_2 films gradually increase and finally approach to those of their bulk counterpart.

3. Conclusion

In summary, we have proposed an innovative two-step method to synthesize wafer-scale, high-quality, and layer-controlled 2D MoS_2 films. Benefitting from sufficient high-quality samples prepared by the proposed method and ultra-broadband (0.73–6.42 eV) SE, the evolution of the dielectric function of MoS_2 ranging from a monolayer to the bulk have been comprehensively investigated. Up to five CPs (A–E) are observed in the broadband dielectric function spectra. These CPs are precisely identified by the CP analysis method, and their physical origins are revealed with the help of the first-principle calculations. The CPs A and B mainly origin from the intralayer SOC effect, and they appear layer-independent with a splitting value of about 150–190 meV. While the CPs C and D correspond to the complex many-body effects, and they exhibit a slightly red-shift as the layer increases with a layer-independent difference value (about 320–380 meV) between them. The formation of the CP E is identified as the direct transitions at the K point of the BZ, and it shows an obvious blue-shift with the layer increasing. Experimental results indicate that the imaginary part of the dielectric functions exhibits a "W" like curve versus the thickness, and the two valley bottoms appear at about four-layer and 10-layer, respectively. These complex layer-dependent fluctuations can be attributed to the alternating domination of the layer-dependent decreasing excitonic effect, the layer-dependent increasing JDOS, and the mass density increase in relative thick MoS_2 specimens.

© 2018 WILEY-VCH Verlag GmbH & Co. KGaA, Weinheim

4. Experimental Section

Preparation of MoS_2: An innovative approach called two-step method was developed to synthetize wafer-scale, high-quality, and layer-controlled 2D MoS_2 films. The ultrathin precursor material of MoO_3 was deposited on a 2 in. size *c*-sapphire wafer from MoO_3 powder with purity of 99.95% (purchased from Gredmann Inc.) by a high-vacuum E-gun evaporator. The thickness of MoO_3 was monitored by a crystal oscillation monitor, which was a main factor in determining the thickness of MoS_2. Then the high-quality MoS_2 film was synthesized by a sulfurization process in a 6 in. furnace with H_2S (10% to Ar gas) as gaseous sulfur source. The formation profile of the temperature was performed by +18 °C min^{-1} ramp up to 750 °C, keeping steady for 60 min then ramp down by −20 °C min^{-1}. The thinnest MoS_2 specimen prepared by the two-step method was three layers when the deposition thickness of MoO_3 was 0.8 nm. To carry out a systematic study on the evolution of the optical property of the MoS_2 versus the thickness, a monolayer continuous MoS_2 film grown directly on a *c*-sapphire by the CVD process and a monocrystalline MoS_2 bulk material (purchased from 2D semiconductor Inc.) were also involved in our experiment.

Characterization of MoS_2: To demonstrate the successful synthesis of MoS_2, an Excalab 250Xi X-ray photoelectron spectrometer with Al-Kα radiation source (1486.6 eV) was used to measure the Mo 3d and S 2p photoelectrons. And the proportion of Mo and S in the film was also evaluated semiquantitatively. The surface roughness and thicknesses of the MoS_2 films were determined by an AFM (Bruker Dimension ICON) and a TEM system (JEOL ARM200F). A commercial SE (ME-L Mueller matrix ellipsometer, Wuhan Eoptics Technology Co., Wuhan, China) was used to investigate the optical property of MoS_2 specimens, whose applicable energy region covers 0.73–6.42 eV.[59,60] The probing spot diameter of the ellipsometer could be as small as 200 µm by using a pair of focusing probes. The microfocusing measurement mode were adopted when measuring the bulk MoS_2 sample, since the relatively flatter area of the bulk MoS_2 could be selectively measured with the help of the microscope attached to the ellipsometer. Multiangle measurement mode was performed to reduce correlations among the fitting parameters, and the incident angles were chosen as 60°, 65°, and 70°.

First-Principle Calculation: In this work, standard ab initio simulations within the density function theory were performed by using of the Vienna Ab initio Simulation Package (VASP v5.4.1),[61] which has been proved to be workable to understand the experimental phenomenon in MoS_2.[62] These calculations were performed using projector augmented wave potentials based on the Perdew–Burke–Ernzerhof[63] exchange-correlation functional within the Heyd–Scuseria–Ernzerhof (HSE) hybrid approach with an exact exchange fraction of 0.25.[64] The vacuum slabs of 15 Å were adopted in the geometric model to avoid interactions between adjacent atom layers. All atomic positions and cell vectors were relaxed with a tolerance of 0.01 eV $Å^{-1}$. Electronic minimization was performed with a tolerance of 10^{-5} eV. An $8 \times 8 \times 1$ grid of k-points was used for the calculations of monolayer MoS_2, while an $8 \times 8 \times 2$ grid was selected to calculate the multilayer MoS_2 samples. The cut-off energies for all MoS_2 samples were set to 550 eV. The calculations included SOC.

Supporting Information

Supporting Information is available from the Wiley Online Library or from the author.

Acknowledgements

B.S. and H.G. contributed equally to this work. This work was funded by the National Natural Science Foundation of China (Grant Nos. 51727809, 51525502, 51805193, and 51775217), the China Postdoctoral Science Foundation (Grant Nos. 2016M602288 and 2017T100546), the National Science and Technology Major Project of China (Grant No. 2017ZX02101006-004), and the National Science Foundation of Hubei Province of China (Grant Nos. 2018CFB559 and 2018CFA057).

Conflict of Interest

The authors declare no conflict of interest.

Keywords

layer-dependent dielectric function, spectroscopic ellipsometry, two-step method, wafer-scale 2D MoS_2

Received: September 12, 2018
Revised: November 1, 2018
Published online: December 3, 2018

[1] Q. Wang, K. K. Zadeh, A. Kis, J. N. Coleman, M. S. Strano, *Nat. Nanotechnol.* **2012**, *7*, 699.
[2] X. Chen, T. Yan, B. Zhu, S. Yang, X. Cui, *ACS Nano* **2017**, *11*, 1581.
[3] S. Manzeli, D. Ovchinnikov, D. Pasquier, O. V. Yazyev, A. Kis, *Nat. Rev. Mater.* **2017**, *2*, 17033.
[4] W. Choi, N. Choudhary, G. H. Han, J. Park, D. Akinwande, Y. H. Lee, *Mater. Today* **2017**, *20*, 116.
[5] J. Ping, Z. Fan, M. Sindoro, Y. Ying, H. Zhang, *Adv. Funct. Mater.* **2017**, *27*, 1605817.
[6] Y. Huang, F. Zhuge, J. Hou, L. Lv, P. Luo, N. Zhou, L. Gan, T. Zhai, *ACS Nano* **2018**, *12*, 4062.
[7] Y. Liu, J. Guo, A. Yu, Y. Zhang, J. Kou, K. Zhang, R. Wen, Y. Zhang, J. Zhai, Z. Wang, *Adv. Mater.* **2018**, *30*, 1704524.
[8] E. Singh, K. S. Kim, G. Y. Yeom, H. S. Nalwa, *ACS Appl. Mater. Interfaces* **2017**, *9*, 3223.
[9] T. Wang, S. Chen, H. Pang, H. Xue, Y. Yu, *Adv. Sci.* **2017**, *4*, 1600289.
[10] K. F. Mak, C. Lee, J. Hone, J. Shan, T. F. Heinz, *Phys. Rev. Lett.* **2010**, *105*, 136805.
[11] T. Cao, G. Wang, W. Han, H. Ye, C. Zhu, J. Shi, Q. Niu, P. Tan, E. Wang, B. Liu, J. Feng, *Nat. Commun.* **2012**, *3*, 1.
[12] B. Radisavljevic, A. Radenovic, J. Brivio, V. Giacometti, A. Kis, *Nat. Nanotechnol.* **2011**, *6*, 147.
[13] C. G. Lee, H. Yan, L. E. Brus, T. F. Heinz, J. Hone, S. M. Ryu, *ACS Nano* **2010**, *4*, 2695.
[14] Y. Li, Y. Rao, K. F. Mak, Y. You, S. Wang, C. R. Dean, T. F. Heinz, *Nano Lett.* **2013**, *13*, 3329.
[15] M. Zhu, K. Huang, K. G. Zhou, *Prog. Cryst. Growth Charact. Mater.* **2017**, *63*, 72.
[16] J. W. Park, H. S. So, S. Kim, S. H. Choi, H. Lee, J. Lee, C. Lee, Y. Kim, *J. Appl. Phys.* **2014**, *116*, 183509.
[17] Y. Yu, Y. Yu, Y. Cai, W. Li, A. Gurarslan, H. Peelaers, D. E. Aspnes, C. G. Van de Walle, N. V. Nguyen, Y. W. Zhang, L. Cao, *Sci. Rep.* **2015**, *5*, 16996.
[18] G. Jia, Y. Liu, J. Gong, D. Lei, D. Wang, Z. Huang, *J. Mater. Chem. C* **2016**, *4*, 8822.
[19] C. Yim, M. O'Brien, N. McEvoy, S. Winters, I. Mirza, J. G. Lunney, G. S. Duesberg, *Appl. Phys. Lett.* **2014**, *104*, 103114.
[20] C. C. Shen, Y. T. Hsu, L. J. Li, H. L. Liu, *Appl. Phys. Express* **2013**, *6*, 125801.
[21] H. L. Liu, C. C. Shen, S. H. Su, C. L. Hsu, M. Y. Li, L. J. Li, *Appl. Phys. Lett.* **2014**, *105*, 201905.
[22] W. Li, A. G. Birdwell, M. Amani, R. A. Burke, X. Ling, Y. H. Lee, X. L. Liang, L. M. Peng, C. A. Richter, J. Kong, D. J. Gundlach, N. V. Nguyen, *Phys. Rev. B* **2014**, *90*, 195434.

 © 2018 WILEY-VCH Verlag GmbH & Co. KGaA, Weinheim

[23] D. Li, X. Song, J. Xu, Z. Wang, R. Zhang, P. Zhou, H. Zhang, R. Huang, S. Wang, Y. Zheng, D. Zhang, L. Chen, *Appl. Surf. Sci.* **2017**, *421*, 884.
[24] S. Funke, B. Miller, E. Parzinger, P. Thiesen, A. W. Holleitner, U. Wurstbauer, *J. Phys.: Condens. Matter* **2016**, *28*, 385301.
[25] G. Jayaswal, Z. Dai, X. Zhang, M. Bagnarol, A. Martucci, M. Merano, *Opt. Lett.* **2018**, *43*, 703.
[26] H. G. Park, T. J. Kim, H. S. Kim, C. H. Yoo, N. S. Barange, V. L. Le, H. U. Kim, V. Senthilkumar, C. T. Le, Y. S. Kim, M. Seong, Y. D. Kim, *Appl. Spectrosc. Rev.* **2016**, *51*, 621.
[27] Y. V. Morozov, M. Kuno, *Appl. Phys. Lett.* **2015**, *107*, 083103.
[28] Y. Li, A. Chernikov, X. Zhang, A. Rigosi, H. M. Hill, A. M. van der Zande, D. A. Chenet, E. Shih, J. Hone, T. F. Heinz, *Phys. Rev. B* **2014**, *90*, 205422.
[29] H. Zhang, Y. Ma, Y. Wan, X. Rong, Z. Xie, W. Wang, L. Dai, *Sci. Rep.* **2015**, *5*, 8440.
[30] B. Mukherjee, F. Tseng, D. Gunlycke, K. K. Amara, G. Eda, E. Simsek, *Opt. Mater. Express* **2015**, *5*, 447.
[31] P. Johari, V. B. Shenoy, *ACS Nano* **2011**, *5*, 5903.
[32] A. Kumar, P. K. Ahluwalia, *Physica B* **2012**, *407*, 4627.
[33] J. Zheng, X. Yan, Z. Lu, H. Qiu, G. Xu, X. Zhou, P. Wang, X. Pan, K. Liu, L. Jiao, *Adv. Mater.* **2017**, *29*, 1604540.
[34] H. Li, Y. Li, A. Aljarb, Y. Shi, L. J. Li, *Chem. Rev.* **2018**, *118*, 6134.
[35] K. S. Novoselov, D. Jiang, F. Schedin, T. J. Booth, V. V. Khotkevich, S. V. Morozov, A. K. Geim, *Proc. Natl. Acad. Sci. USA* **2005**, *102*, 10451.
[36] A. Jawaid, D. Nepal, K. Park, M. Jespersen, A. Qualley, P. Mirau, L. F. Drummy, R. A. Vaia, *Chem. Mater.* **2016**, *28*, 337.
[37] Y. Peng, Z. Meng, C. Zhong, J. Lu, W. Yu, Y. Jia, Y. Qian, *Chem. Lett.* **2001**, *30*, 772.
[38] C. Tan, X. Cao, X. J. Wu, Q. He, J. Yang, X. Zhang, J. Chen, W. Zhao, S. Han, G. H. Nam, M. Sindoro, H. Zhang, *Chem. Rev.* **2017**, *117*, 6225.
[39] Y. H. Lee, X. Q. Zhang, W. Zhang, M. T. Chang, C. T. Lin, K. D. Chang, Y. C. Yu, J. T. Wang, C. S. Chang, L. J. Li, T. W. Lin, *Adv. Mater.* **2012**, *24*, 2320.
[40] Q. A. Vu, H. Kim, V. L. Nguyen, U. Y. Won, S. Adhikari, K. Kim, Y. H. Lee, W. J. Yu, *Adv. Mater.* **2017**, *29*, 1703363.
[41] Z. Lin, Y. Zhao, C. Zhou, R. Zhong, X. Wang, Y. H. Tsang, Y. Chai, *Sci. Rep.* **2016**, *5*, 18596.
[42] N. Liu, P. Kim, J. H. Kim, J. H. Ye, S. Kim, C. J. Lee, *ACS Nano* **2014**, *8*, 6902.
[43] A. Chernikov, T. C. Berkelbach, H. M. Hill, A. Rigosi, Y. L. Li, O. B. Aslan, D. R. Reichman, M. S. Hybertsen, T. F. Heinz, *Phys. Rev. Lett.* **2014**, *113*, 076802.
[44] P. Y. Yu, M. Cardona, *Fundamentals of Semiconductors Physics and Materials Properties*, Springer, Berlin, Heidelberg, Germany **2010**.
[45] O. S. Heavens, *Optical Properties of Thin Solid Films*, Dover, New York, USA **1991**.
[46] Y. T. Ho, C. H. Ma, T. T. Luong, L. L. Wei, T. C. Yen, W. T. Hsu, W. H. Chang, Y. C. Chu, Y. Y. Tu, K. P. Pande, E. Y. Chang, *Phys. Status Solidi RRL* **2015**, *9*, 187.
[47] K. K. Liu, W. Zhang, Y. H. Lee, Y. C. Lin, M. T. Chang, C. Y. Su, C. S. Chang, H. Li, Y. Shi, H. Zhang, C. S. Lai, L. J. Li, *Nano Lett.* **2012**, *12*, 1538.
[48] D. E. Aspnes, J. B. Theeten, *Phys. Rev. B* **1979**, *20*, 3292.
[49] *Ellipsometry at the Nanoscale* (Eds: M. Losurdo, K. Hingerl), Springer-Verlag, Berlin, Heidelberg, Germany **2013**.
[50] J. A. Wilson, A. D. Yoffe, *Adv. Phys.* **1969**, *18*, 193.
[51] A. M. Sánchez, D. Sangalli, K. Hummer, A. Marini, L. Wirtz, *Phys. Rev. B* **2013**, *88*, 045412.
[52] D. W. Latzke, W. Zhang, A. Suslu, T. R. Chang, H. Lin, H. T. Jeng, S. Tongay, J. Wu, A. Bansil, A. Lanzara, *Phys. Rev. B* **2015**, *91*, 235202.
[53] T. Cheiwchanchamnangij, W. R. L. Lambrecht, *Phys. Rev. B* **2012**, *85*, 205302.
[54] D. Y. Qiu, F. H. da Jornada, S. G. Louie, *Phys. Rev. Lett.* **2013**, *111*, 216805.
[55] E. Ridolfi, C. H. Lewenkopf, V. M. Pereira, *Phys. Rev. B* **2018**, *97*, 205409.
[56] A. Kuc, N. Zibouche, T. Heine, *Phys. Rev. B* **2011**, *83*, 245213.
[57] X. Fan, D. J. Singh, W. Zheng, *J. Phys. Chem. Lett.* **2016**, *7*, 2175.
[58] H. Fujiwara, *Spectroscopic Ellipsometry: Principles and Applications*, John Wiley & Sons, Chichester, West Sussex, England **2007**.
[59] S. Liu, X. Chen, C. Zhang, *Thin Solid Films* **2015**, *584*, 176.
[60] B. Song, H. Gu, S. Zhu, H. Jiang, X. Chen, C. Zhang, S. Liu, *Appl. Surf. Sci.* **2018**, *439*, 1079.
[61] G. Kresse, J. Furthmüller, *Phys. Rev. B* **1996**, *54*, 11169.
[62] T. Chu, H. Ilatikhameneh, G. Klimeck, R. Rahman, Z. Chen, *Nano Lett.* **2015**, *15*, 8000.
[63] J. P. Perdew, K. Burke, M. Ernzerhof, *Phys. Rev. Lett.* **1996**, *77*, 3865.
[64] A. V. Krukau, O. A. Vydrov, A. F. Izmaylov, G. E. Scuseria, *J. Chem. Phys.* **2006**, *125*, 224106.

© 2018 WILEY-VCH Verlag GmbH & Co. KGaA, Weinheim

Copyright WILEY-VCH Verlag GmbH & Co. KGaA, 69469 Weinheim, Germany, 2018.

ADVANCED OPTICAL MATERIALS

Supporting Information

for *Advanced Optical Materials,* DOI: 10.1002/adom.201801250

Layer-Dependent Dielectric Function of Wafer-Scale 2D MoS_2

Baokun Song, Honggang Gu, Mingsheng Fang, Xiuguo Chen, Hao Jiang, Renyan Wang, Tianyou Zhai, Yen-Teng Ho,* and Shiyuan Liu**

Supporting Information

Layer-dependent dielectric function of wafer-scale 2D MoS_2

Baokun Song,‡ Honggang Gu,‡ Mingsheng Fang, Xiuguo Chen, Hao Jiang, Renyan Wang, Tianyou Zhai*, Yen-Teng Ho*, and Shiyuan Liu*

B. K. Song, Dr. H. G. Gu, M. S. Fang, Dr. X. G. Chen, Dr. H. Jiang, Prof. S. Y. Liu

State Key Laboratory of Digital Manufacturing Equipment and Technology, Huazhong University of Science and Technology, Wuhan 430074, Hubei, China.
E-mail: shyliu@hust.edu.cn

R. Y. Wang, Prof. T. Y. Zhai
State Key Laboratory of Material Processing and Die and Mould Technology, Huazhong University of Science and Technology, Wuhan 430074, Hubei, China.
E-mail: zhaity@hust.edu.cn

Prof. Y. T. Ho
Department of Materials Science and Engineering, National Chiao Tung University, Hsinchu 30010, Taiwan, China.
E-mail: 9418813@gmail.com

‡ These authors contributed equally to the work.

AFM

Figure S1 illustrates the surface roughness and thicknesses of the MoS_2 specimens (1L, 6L, 8L, 13L) measured by AFM. The scanned area in the AFM measurements is 1μm×1μm for these MoS_2 specimens except for the 13-layers MoS_2, whose measured area is 10μm×10μm (leads to a higher R_q value).

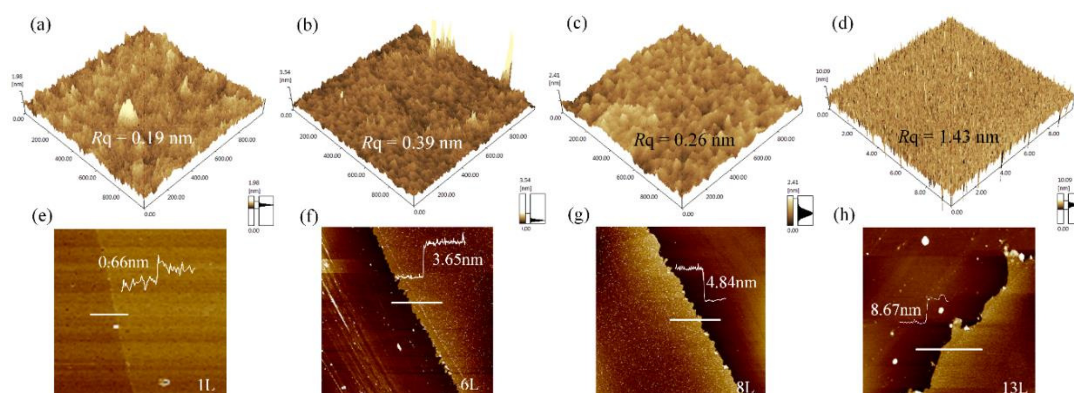

Figure S1. AFM results for MoS_2 films.

Optical micrograph of bulk MoS_2

The surface conditions of the high quality bulk MoS_2 crystal (purchased from the 2D semiconductor Inc.) used in our experiment was checked by an optical microscope (OM). As shown in the optical micrograph Figure S2, the bulk MoS_2 has a smooth surface over a large area, which provides a lot of convenience to perform reliable ellipsometric measurement.

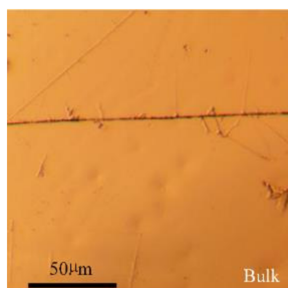

Figure S2. An optical micrograph of the bulk MoS_2 sample.

Ellipsometric analysis

In the ellipsometric analysis, a layer-stack model (Figure S3) was constructed to describe the optical structure of 2D MoS_2 film on c-sapphire, which contains four layers including the surrounding medium (air) layer, the MoS_2 thin film layer, a Bruggeman interlayer containing 50% MoS_2 and 50% c-sapphire, and the c-sapphire substrate. It is worth noting that the Bruggeman interlayer can effectively describe the transition interface between two materials.[1] By introducing the Bruggeman interlayer, the goodness of the ellipsometric fit can be further improved.[2,3] To physically embody the dielectric properties of MoS_2 over the concerned broadband range, the dielectric functions are parameterized by a combination of classical oscillators, including a Cody-Lorentz oscillator and five Lorentz oscillators.[1,4,5] The specific mathematical expressions for the above two kinds of oscillators can be found in references 5 and 1. With the established optical model and the parameterized dielectric functions, the theoretical ellipsometric spectra (Ψ(E), Δ(E)) of the MoS_2 can be calculated by the

transfer matrix method.[1] Then, the dielectric functions and thicknesses of the MoS_2 films can be extracted by fitting the measured ellipsometric spectra with theoretically calculated ones. Further details on the ellipsometric analysis can refer to our previous publication[6] and some other representative works.[7-9]

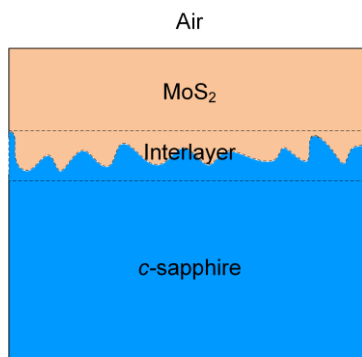

Figure S3. Optical model of MoS_2 film on c-sapphire

The ellipsometric analysis results for the MoS_2 samples have been shown in Figure S4. It can be seen that for all the test samples, the best fitting ellipsometric spectra (Ψ (E), Δ (E)) exhibit high agreement with the measured ones, demonstrating the correctness of our ellipsometric analysis.

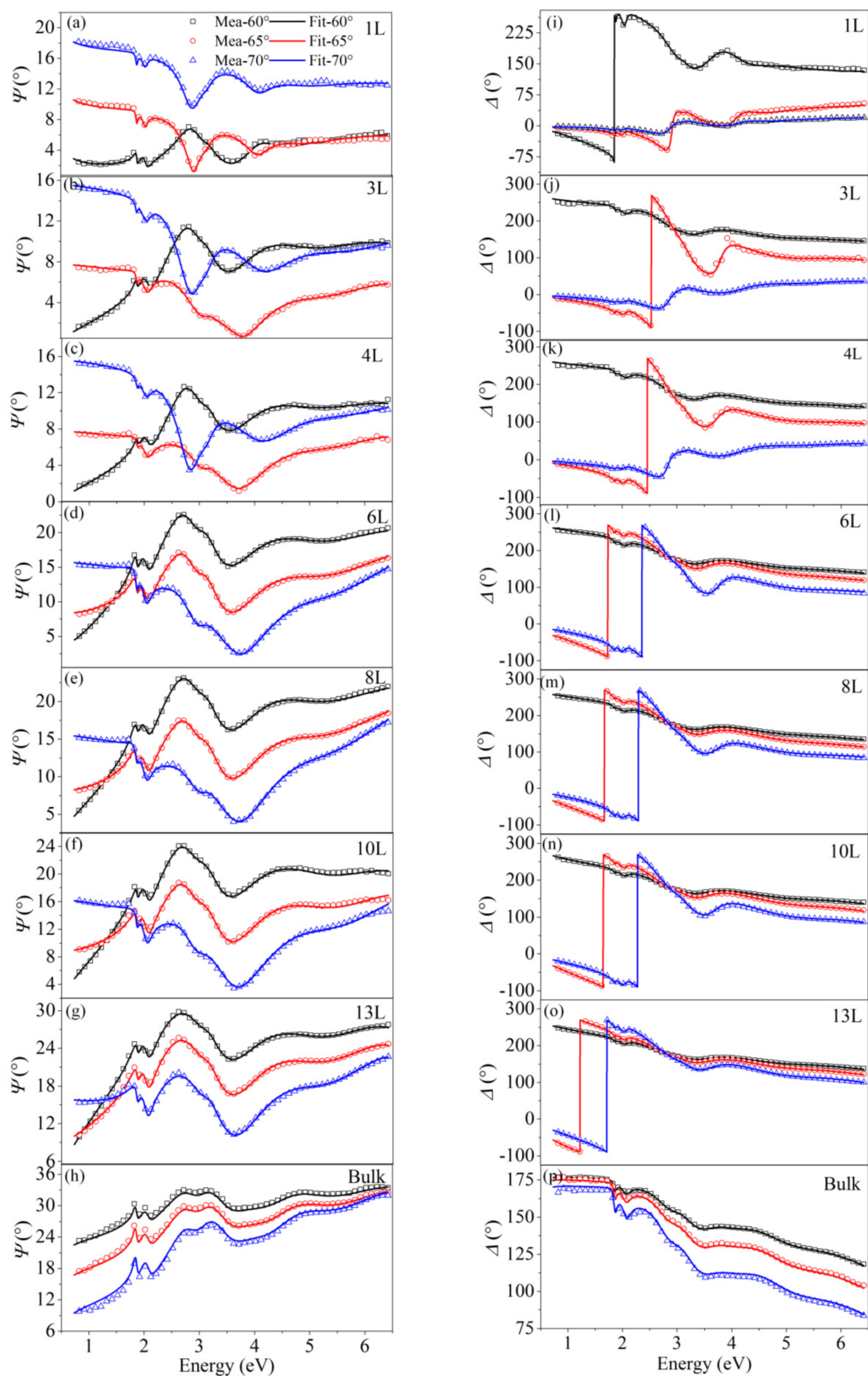

Figure S4. The measured and best fitting ellipsometric spectra of the MoS_2 samples.

Critical point (CP) analysis method

In the CP analysis method, the second derivative of the dielectric function spectra are fitted by theoretical formulas as given by

$$d^2\varepsilon / dE^2 = \begin{cases} m(m-1)\,A\exp(i\phi)(E - E_0 + i\Gamma)^{n-2} & (m \neq 0) \\ A\exp(i\phi)(E - E_0 + i\Gamma)^{-2} & (m = 0) \end{cases}, \quad (S1)$$

where the adjustable parameters A, ϕ, E_0, and Γ represent the amplitude, the phase, the center energy, and the damping coefficient of the CP, respectively, and m refers to the dimension of the wave vector. The excitonic lineshape ($m = -1$), is a fine description of the optical transitions at these CPs.[10] The second derivatives of the dielectric functions illustrated in Figure 3 and the best fitting curves have been presented in Figure S5. The parameters corresponding to the best fitting results are summarized in Table S1, and the center energies of the above CPs agree very well with previous experimental findings[10] and theoretical predications.[11,12] It can be seen that the positions as well as the shapes of these CPs can be totally determined by the CP analysis method.

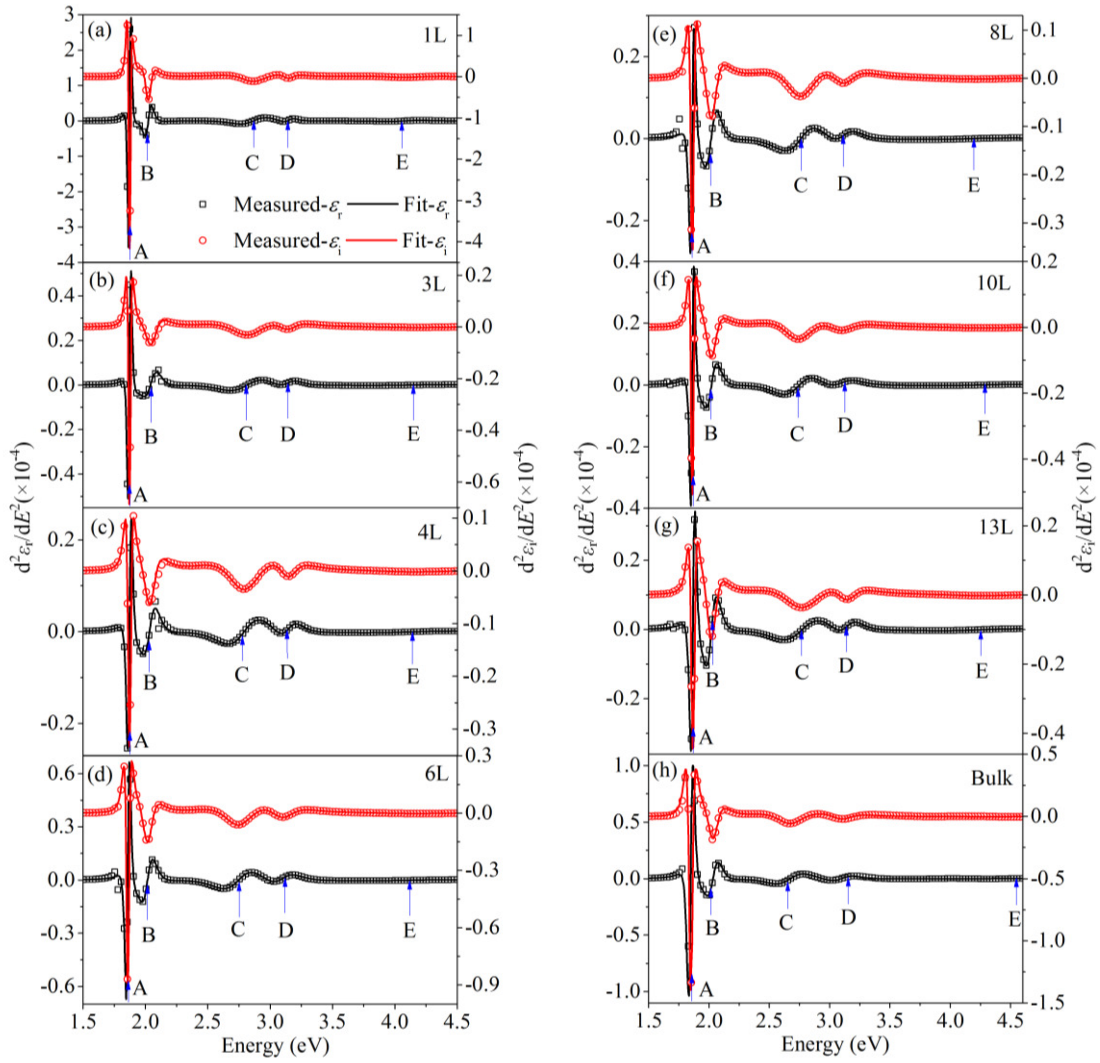

Figure S5. The measured and best fitting second derivative spectra of the dielectric functions of MoS_2 samples.

Table S1. Best fitting parameters of the CPs analysis for the MoS_2 samples.

Parameters	CPs	1L	3L	4L	6L	8L	10L	13L	Bulk
A (no unit)	A	0.22	0.06	0.07	0.16	0.09	0.08	0.14	0.53
	B	0.60	0.54	0.46	0.78	0.61	0.56	0.69	1.09
	C	8.74	5.67	5.23	7.54	5.51	5.03	9.37	5.85
	D	0.39	0.42	0.46	1.93	1.18	1.68	0.72	1.62
	E	2.80	5.28	4.44	4.86	3.73	4.37	6.27	3.50
ϕ (°)	A	160.00	160.22	160.21	166.53	160.24	160.22	160.22	160.19
	B	172.80	173.02	172.91	172.84	172.86	172.78	172.78	172.95
	C	128.81	128.78	128.76	128.81	128.83	128.73	128.70	128.77
	D	153.90	153.96	153.93	153.97	154.05	153.96	153.91	154.02
	E	279.51	279.59	279.52	279.28	279.66	279.68	279.56	280.55
E_0 (eV)	A	1.87	1.87	1.87	1.86	1.86	1.86	1.87	1.85
	B	2.02	2.05	2.04	2.02	2.02	2.02	2.02	2.04
	C	2.87	2.82	2.79	2.75	2.76	2.74	2.76	2.67
	D	3.15	3.14	3.14	3.10	3.12	3.09	3.14	3.10
	E	4.07	4.16	4.13	4.11	4.21	4.28	4.25	4.55
Γ (eV)	A	0.02	0.03	0.03	0.03	0.04	0.03	0.04	0.04
	B	0.06	0.11	0.11	0.10	0.11	0.11	0.10	0.10
	C	0.25	0.32	0.31	0.28	0.30	0.29	0.36	0.27
	D	0.10	0.17	0.17	0.22	0.23	0.26	0.18	0.22
	E	0.30	0.76	0.76	0.70	0.70	0.75	0.75	0.82

References

[1] H. Fujiwara, Spectroscopic Ellipsometry: Principles and Applications, John Wiley & Sons, Chichester, West Sussex, England, **2007**.

[2] D. E. Aspnes, J. B. Theeten, Phys. Rev. B **1979**, 20, 3292-3302.

[3] M. Losurdo, K. Hingerl, Eds., Ellipsometry at the Nanoscale, Springer-Verlag, Berlin, Heidelberg, Germany **2013**.

[4] C. C. Shen, Y. T. Hsu, L. J. Li, H. L. Liu, Appl. Phys. Express **2013**, 6, 125801.

[5] A. S. Ferlauto, G. M. Ferreira, J. M. Pearce, C. R. Wronski, R. W. Collins, X. Deng, G. Ganguly, J. Appl. Phys. **2002**, 92, 2424-2436.

[6] B. Song, H. Gu, S. Zhu, H. Jiang, X. Chen, C. Zhang, S. Liu, Appl. Surf. Sci. **2018**, 439, 1079-1087.

[7] M. Shirayama, H. Kadowaki, T. Miyadera, T. Sugita, M. Tamakoshi, M. Kato, T. Fujiseki, D. Murata, S. Hara, T. N. Murakami, S. Fujimoto, M. Chikamatsu, H. Fujiwara, **2016**, 5, 014012.

[8] A. M. A. Leguy, P. Azarhoosh, M. L. Alonso, M. Campoy-Quiles, O. J. Weber, J. Yao, D. Bryant, M. T. Weller, J. Nelson, A. Walsh, M. V. Schilfgaarde, P. R. F. Barnes, Nanoscale **2016**, 8, 6317-6327.

[9] F. J. Nelson, V. K. Kamineni, T. Zhang, E. S. Comfort, J. U. Lee, A. C. Diebold, Appl. Phys. Lett. **2010**, 97, 253110.

[10] W. Li, A. G. Birdwell, M. Amani, R. A. Burke, X. Ling, Y. H. Lee, X. L. Liang, L. M. Peng, C. A. Richter, J. Kong, D. J. Gundlach, N. V. Nguyen, Phys. Rev. B **2014**, 90, 195434.

[11] A. M. Sánchez, D. Sangalli, K. Hummer, A. Marini, L. Wirtz, Phys. Rev. B **2013**, 88, 045412.

[12] D. W. Latzke, W. Zhang, A. Suslu, T. R. Chang, H. Lin, H. T. Jeng, S. Tongay, J. Wu, A. Bansil, A. Lanzara, Phys. Rev. B **2015**, 91, 235202.